

# Shadow surface states in topological Kondo insulators

Areg Ghazaryan,<sup>1</sup> Emilian M. Nica,<sup>2</sup> Onur Erten,<sup>2</sup> and Pouyan Ghaemi<sup>3,4</sup>

<sup>1</sup>*IST Austria (Institute of Science and Technology Austria), Am Campus 1, 3400 Klosterneuburg, Austria*

<sup>2</sup>*Department of Physics, Arizona State University Tempe, Arizona 85287-1504, US*

<sup>3</sup>*Physics Department, City College of the City University of New York, New York, NY 10031, USA*

<sup>4</sup>*Physics Program, Graduate Center of the City University of New York, NY 10031, USA*

The surface states of 3D topological insulators can exhibit Fermi surfaces of arbitrary area when the chemical potential is tuned away from the Dirac points. We focus on topological Kondo insulators and show that the surface states can acquire a finite Fermi surface even when the chemical potential is pinned to the Dirac point energy. We illustrate how this can occur when the crystal symmetry is lowered from cubic to tetragonal in a minimal two-orbital model. We label such surface modes as ‘shadow surface states’. We also show that for certain bulk hybridization the Fermi surface of the shadow states can become comparable to the extremal area of the unhybridized bulk bands. The ‘large’ Fermi surface of the shadow states is expected to lead to large-frequency quantum oscillations in the presence of an applied magnetic field. Consequently, shadow surface states provide an alternative to mechanisms involving bulk Landau-quantized levels or surface Kondo breakdown for anomalous magnetic quantum oscillations in topological Kondo insulators with tetragonal crystal symmetry.

## I. INTRODUCTION

Kondo insulators are strongly correlated systems where the hybridization between the quasi-localized  $f$ -electrons and the itinerant conduction electrons leads to an insulating gap at low temperatures<sup>1</sup>. The archetypal Kondo insulator  $\text{SmB}_6$ , discovered over 50 years ago<sup>2</sup>, drew revived interest with proposals advancing topological surface states as an explanation for the previously-reported low-temperature resistivity plateau<sup>3–6</sup>. While angle-resolved photoemission spectroscopy (ARPES) experiments have since resolved these topological surface states<sup>7–12</sup> a number of puzzles remain, most notably in the linear specific heat with a large Sommerfeld coefficient<sup>13</sup>, gapless optical conductivity<sup>14</sup> and unconventional quantum oscillations<sup>15–18</sup> (QO). Although specific heat and optical conductivity anomalies most likely originate from the bulk of  $\text{SmB}_6$ , the nature of the QO is still under debate. Similar unconventional QO have also been observed in another Kondo insulator  $\text{YbB}_{12}$ <sup>19,20</sup>, suggesting a unified underlying mechanism. Several theoretical proposals based on magnetic breakdown<sup>21</sup>, excitons<sup>22</sup>, impurity bands<sup>23</sup>, fractionalization<sup>24–27</sup> and surface driven mechanisms<sup>28,29</sup> have been advanced in this context.

A key aspect of QO experiments in  $\text{SmB}_6$  is the observation of large frequency oscillations which apparently match the extremal area of the unhybridized bulk bands. This naturally suggests that the bulk Landau-quantized states underpin the observed oscillations. However, ARPES experiments<sup>7–12</sup> on  $\text{SmB}_6$  indicate a surface-state Fermi surface (FS) with total area which is comparable to the extremal area of the unhybridized bands, which raises the possibility that large QO frequencies are instead rooted in the surface states. Surface Kondo breakdown<sup>28,29</sup> has been proposed as one possible mechanism for the emergence of a ‘large’ FS for the surface states: the Kondo effect is suppressed on the surface,

liberating the conduction electrons which contribute directly to the FS of the surface states which expands as a consequence.

On another front, we now know that surface states of symmetry-protected topological phases can have structures beyond typical 2D Dirac bands. Better-known examples are hexagonal warped surface states<sup>30</sup> or corner states of higher-order topological insulators<sup>31</sup>. The surface states emerge due to the bulk band structure rather than the surface effects. It is then natural to ask whether topological surface states with FSs with an area which is comparable to the extremal area of the unhybridized bulk bands can result from certain bulk band structures.

In most two-orbital models of non-interacting topological insulators (TIs), the bulk band structure and gap are determined by the direct hybridization between electrons in different orbitals. By contrast, in a minimal two-orbital model for TKIs<sup>28</sup>, the effective hybridization between the orbitals, which leads to a finite gap, can be traced to the Kondo screening, at mean-field level. Consequently, the gap structure and the surface states in TKIs are not determined simply by the overlap of the weakly-interacting orbitals, but rather emerge as a consequence of Kondo interactions, and thus can exhibit a wider array of possible structures.

As we illustrate, surface states with ‘large’ FSs can emerge in TKIs due to additional next-nearest neighbor (NNN) effective hybridization terms, which are consistent with the tetragonal point-group symmetry and with the Kondo-screened nature of the ground-state. We refer to these as ‘shadow surface states’.

The shadow FS results from the structure of the bulk gap which supports gapless surface states for arbitrary finite momentum around the surface Brillouin Zone (BZ) center. This regime can be accessed by tuning the anisotropy of the NNN hybridization from cubic to tetragonal. Correspondingly, the surface-state FS undergoes multiple Lifshitz transitions tuned by modification

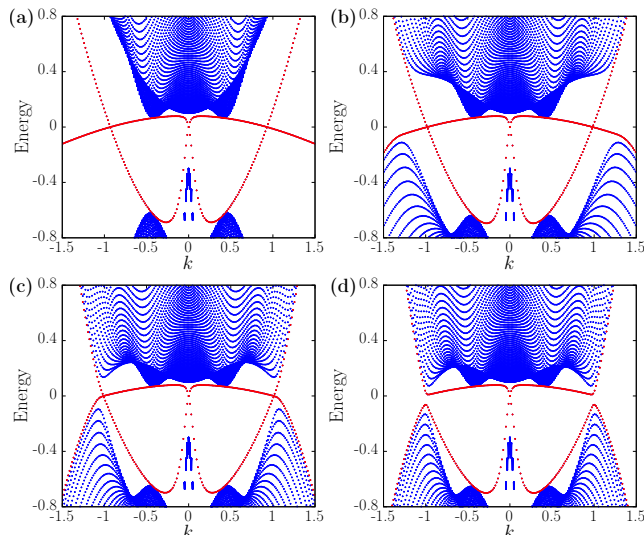


FIG. 1. Evolution of the spectrum of a two-orbital model for topological Kondo insulators in the presence of NN and NNN hybridization terms with tetragonal symmetry. The panels correspond to solutions with decreasing tetragonal anisotropy, as determined by the parameter  $\beta$  in (3). Blue and red points denote surface and bulk states, respectively. The momentum  $k$  is chosen along the  $\Gamma$  to  $M$  direction ( $\theta_k = \pi/4$ ). Panel (a) ( $\beta = 0$ ) illustrates the emergence of shadow states. The second crossing of the two surface bands also occurs for finite momenta along an arbitrary in-plane axis, signaling the presence of a finite FS. Panels (b-d), corresponding to  $\beta = 0.2, 0.3$  and  $0.35$  respectively, illustrate the presence and gapping of Dirac points. The associated Lifshitz transitions are discussed in the text. The numerical solutions were obtained for a slab geometry using a lattice model corresponding to  $H_T$  in (1) with open boundary conditions and 200 lattice sites along the  $z$  direction. The parameters of the model are  $M' = m' = -0.45$ ,  $M = m = -0.55$ ,  $v = 1.0$  and  $\alpha = -6.0$ .

of the crystal symmetry. Shadow states and the corresponding finite FS emerge strictly for in-plane only NNN hybridization. For small but finite out-of-plane NNN hybridization, a non-uniform gap opens everywhere on the shadow FS with the exception of 8 points. As the out-of-plane NNN hybridization increases, 4 of these Dirac points become gapped.

The TKI mean field model, with additional NNN coupling, retains a strong topological insulator classification upon lowering the point-group symmetry from cubic to tetragonal, as indicated by the changes in the surface-state spectrum. For general NNN hybridization anisotropy, an even number of additional Dirac points appear in the surface-state spectrum. When shadow states with a finite FS emerge, the chemical potential intersects the surface-state bands at an odd number of points along any axis extending from the center of the BZ, as shown in Fig. (1) (a) along  $\Gamma$ - $M$ .

We further show that the relative strength of NNN and nearest-neighbor (NN) hybridization controls the size of the shadow state FS, which approaches the ex-

tremal area of the unhybridized bands for specific value of parameters. In these cases, shadow states provide an alternative to previously-proposed mechanisms underlying large-frequency QO which involve the bulk Landau-levels or surface Kondo breakdown. Although a finite gap opens along the surface-state FS for any finite out-of-plane NNN hybridization, as previously discussed, we expect its effect on the QO is negligible as long as the Landau level spacing is larger than the surface gap. While not immediately applicable to the anomalous QO in cubic  $\text{SmB}_6$ , shadow states can also become natural candidates in cases where the symmetry is lowered via application of uniaxial strain.

The rest of the paper is organized as follows. In Sec. II, we introduce effective non-interacting models for topological Kondo insulators with tetragonal symmetry and illustrate the emergence of shadow surface states in analytical and numerical solutions of the models. In Sec. III, we consider the Kondo interactions corresponding to the effective models in Sec. II. We show that the minimum-energy self-consistent saddle-point solutions lead to the emergence of shadow states. A detailed derivation of the analytical solutions of the the effective models introduced in Sec. II is presented in the Appendix.

## II. SHADOW SURFACE STATES

The minimal, two-orbital model for cubic 3D topological insulators (TI) in the continuum limit has the form<sup>32-35</sup>

$$H_0 = (M' - m'k^2) \tau_0 + (M - mk^2) \tau_z + v\mathbf{k} \cdot \boldsymbol{\sigma} \tau_x, \quad (1)$$

where  $\tau$  ( $\sigma$ ) acts on the orbital (spin) basis. We choose units where the lattice constant  $a = 1$ .  $H_0$  also describes the effective mean-field Hamiltonian for topological Kondo Insulators (TKIs)<sup>6,28</sup>. In most minimal models of TKIs, the narrow band originates from quasi-localized  $p$  orbitals while the wide band is due to the itinerant  $s$  orbital conduction electrons, mimicking the  $f$  and  $d$  orbitals in real materials. In contrast to conventional TIs such as  $\text{Bi}_2\text{Se}_3$ , the gap in TKIs emerges due to the Kondo interactions, taken at mean-field level. The nature of the insulating state depends on the sign of the product of the two mass terms with  $Mm > 0$  ( $Mm < 0$ ) for strong topological or trivial insulators, respectively. The Fermi energy of the bulk unhybridized gapless bands ( $v = 0$ ) is determined by  $E_f = M' - \frac{m'}{m}M$  corresponding to the energy where the two bands cross at momentum  $k_F = \sqrt{M/m}$ . An insulating gap appears as the hybridization  $v$  is turned on, provided that  $|m'| < m$ . Furthermore, we consider cases where  $Mm > 0$  such that the gapped phase corresponds to a strong TI. The indirect gap closes when  $m = m'$  and for  $|m'| > m$  the system transitions to a metallic state. We introduce boundary surfaces chosen for convenience to be perpendicular to the  $z$  axis. In the strong TI phase, the dispersion of

the surface states can be derived following the standard procedure<sup>32,36,37</sup>

$$E_{\pm}^0 = E_f \pm vk_{\parallel} \sqrt{1 - \left(\frac{m'}{m}\right)^2}, \quad (2)$$

where  $k_{\parallel} = \sqrt{k_x^2 + k_y^2}$ . Without loss of generality, we consider the case where the chemical potential for the surface states coincides with the bulk Fermi energy  $E_f$ . The surface bands cross the Fermi energy at  $k_{\parallel} = 0$ , corresponding to a 2D Dirac point.

We now consider additional point-group symmetry-allowed NNN hybridization terms in the continuum limit:

$$V_{nnn} = \alpha v \left[ k_x (\beta k_y^2 + k_z^2) \sigma_x + k_y (\beta k_x^2 + k_z^2) \sigma_y + k_z (k_x^2 + k_y^2) \sigma_z \right] \tau_x. \quad (3)$$

Note that the  $\mathbf{k} \cdot \sigma$  hybridization in (1) as well as  $V_{nnn}$  are the limiting forms of NN and NNN hybridizations in a lattice model which preserves the  $O_h$  cubic point-group symmetry, respectively, as shown in Sec III.  $|\alpha|$ , which was introduced in  $V_{nnn}$ , controls the relative strength of the NNN/NN hybridization. Importantly, we have generalized the cubic-symmetry allowed NNN terms to allow for tetragonal anisotropy corresponding to  $D_{4h}$  point-group symmetry, by introducing the anisotropy factors  $\beta$ . Indeed,  $\beta = 1$  and  $\beta \neq 1$  correspond to cubic and tetragonal point-groups, respectively. Although the Hamiltonian in (1) should also reflect the tetragonal anisotropy we find that neglecting this does not qualitatively affect our results.

We now consider the Hamiltonian  $H_T = H_0 + V_{nnn}$ , which includes the NNN hybridization terms.  $H_T$  supports surface states as shown in the Appendix. To understand the structure of these states, we first consider the case with maximal tetragonal anisotropy corresponding to  $\beta = 0$ . The surface state dispersion reads:

$$E_{\pm} = \frac{M'm^2 - Mmm'}{m^2 + \alpha^2 v^2 k_{\parallel}^2} + \frac{\alpha v^2 \left[ m'k_{\parallel}^2 + \alpha \left( M' - m'k_{\parallel}^2 \right) k_{\parallel}^2 \right]}{m^2 + \alpha^2 v^2 k_{\parallel}^2} \pm \frac{vk_{\parallel} \left| m + \alpha \left( M - mk_{\parallel}^2 \right) \right|}{m^2 + \alpha^2 v^2 k_{\parallel}^2} \sqrt{m^2 - (m')^2 + \alpha^2 v^2 k_{\parallel}^2}. \quad (4)$$

where  $k_{\parallel}$  is the momentum in the radial direction. In contrast to (1) where the two surface-state bands cross only at the Dirac point for  $k_{1,\parallel} = 0$ , the presence of the additional bulk NNN hybridization in (3) leads to additional crossings of the two surface-state bands at radial momenta  $k_{2,\parallel} = \sqrt{M/m + 1/\alpha}$ . To understand why the additional crossings on the circle of radius  $k_{2,\parallel}$  occur, we examine the real-space representation of  $H_T$  with open boundary conditions along  $z$  and  $\beta = 0$ :

$$H_T = (M' - m'k_x^2 + m'\partial_z^2) \tau_0 + (M - mk_x^2 + m^2\partial_z^2) \tau_z + v \left[ k_x (1 - \alpha\partial_z^2) \sigma_x - i\partial_z (1 + \alpha k_x^2) \sigma_z \right]. \quad (5)$$

The hybridization part of the Hamiltonian (5) which is proportional to  $v$  has the structure of the Su-Schrieffer-Heeger Hamiltonian<sup>38</sup> and has a zero-energy edge state when  $\alpha < 0$  for any  $k_x$ . This edge state not being sensitive to the presence of the bulk gap hints at the possibility that the Hamiltonian (5) has edge states with properties which resemble the bulk band structure when the bulk gap is closed. The condition for the presence of surface states at  $E_f$  and non-zero momentum  $k_{2,\parallel}$  can be directly deduced from the full Hamiltonian  $H_T$ . We require two non-trivial eigenstates with the same sign decay lengths to satisfy the open boundary condition<sup>32</sup>. As outlined in the Appendix, the decay lengths of the two in-gap eigenstates of the Hamiltonian must satisfy

$$\lambda_1 \lambda_2 = -\frac{1}{\alpha}, \quad (6)$$

which implies  $\alpha < 0$ . We further require that the radial momentum of the additional crossing  $k_{2,\parallel} = \sqrt{M/m + 1/\alpha}$  be real which implies the following condition for the emergence of edge states with finite size FS:

$$\alpha < -m/M. \quad (7)$$

In addition, with increasing  $|\alpha|$ ,  $k_{2,\parallel}$  approaches the radius of the extremal area of the bulk unhybridized bands. In these cases, surface states which cross the Fermi energy at large momentum  $k_{2,\parallel}$  are expected to lead to magnetic oscillations with a large frequency, which in many ways resemble the QO from the bulk Landau-levels or surface Kondo breakdown.

We illustrate these arguments via a comparison between the analytical solutions of  $H_T$  in the continuum limit and the numerical solution of a lattice tight-binding model corresponding to  $H_T$  discussed in detail in the next section. The results are summarized in Fig. 1 (a) and Fig. 2. Fig. 1 (a) shows the dependence of the lowest energy states of  $H_T$  in a slab geometry with surfaces normal to the  $\hat{z}$  direction.

The surface states clearly show two crossings at  $k_{1,\parallel} = 0$  and at finite momentum  $k_{2,\parallel}$ . Fig. 2 (a) shows the dependence of  $k_{2,\parallel}$  on  $\alpha$  obtained from the formula presented above and from the tight binding equivalent of  $H_T$ , respectively. The numerical and analytical results are in close agreement and, for  $\alpha < -6$ , the surface state FS approaches the extremal surface of the bulk unhybridized bands, whenever the gap vanishes, as illustrated in Fig. 2 (b).

For  $\beta = 0$ , the FS, which is circularly symmetric for the chosen parameters with radius  $k_{2,\parallel}$ , corresponds to the crossing points of the two surface bands. For non-zero  $\beta$ , a gap opens on the surface-state FS, except for 8

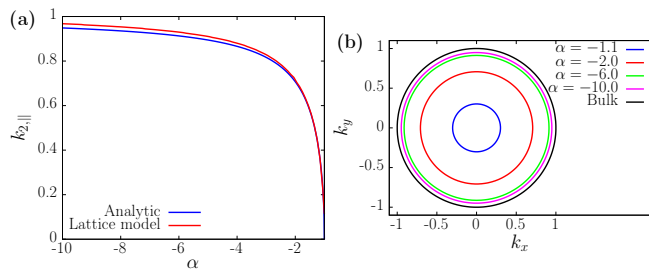


FIG. 2. (a) Radius of shadow state Fermi circle  $k_{2,||}$  versus the NNN hybridization strength  $\alpha$  as determined from the numerical and analytical solutions of  $H_T$ . (b) Evolution of the shadow state FS with  $\alpha$ . The black line corresponds to the extremal-area section of the FS for the bulk unhybridized bands. For sufficiently large  $\alpha$ , the shadow state FS becomes comparable to the extremal area of the bulk unhybridized bands. The shadow state solutions were obtained for  $\beta = 0$  and all remaining parameters are the same as in Fig. 1.

points located at  $\theta_k = m\pi/2$  and  $\theta_k = \pi/4 + m\pi/2$  ( $m$  is integer and  $\tan \theta_k = k_y/k_x$ ). These correspond to surface Dirac points. We distinguish between Dirac points at  $\theta_k = m\pi/2$  and  $\theta_k = \pi/4 + m\pi/2$ . For  $\theta_k = m\pi/2$  the Dirac points are located at  $k_{2,||} = \sqrt{M/m + 1/\alpha}$  (since  $\beta$  dependent terms do not contribute when either  $k_x$  or  $k_y$  is zero), while for  $\theta_k = \pi/4 + m\pi/2$  the Dirac points occur at  $k'_{2,||} = \sqrt{(m + M\alpha)/m\alpha(1 - \beta/2)}$ . As  $\beta$  increases beyond a critical value  $\beta_c = 2/|\alpha|k_F^2 = 2m/|\alpha|M$ , the *bulk* gap closes for  $\theta_k = \pi/4 + m\pi/2$  and the corresponding *surface* Dirac points become gapped. This is confirmed by the numerical results shown in Fig. 1 (b-d). At  $\beta = \beta_c$  the bulk band structure contains four 3D Dirac points located in the  $k_z = 0$  plane, along directions  $\theta_k = \pi/4 + m\pi/2$  and at distance  $k_F$  from the center of the BZ as shown in Fig. 3. For  $\beta > \beta_c$  the FS of the surface state consists of four Fermi points at directions  $\theta_k = m\pi/2$ .

Fig. 4 shows the evolution of the surface-state band gap and corresponding FS extracted from the numerical solutions as a function of  $\beta$ . There are two Lifshitz transitions between the bands in panels (a) and (b) and (c) and (d), respectively, as the point-group symmetry is enhanced from tetragonal to cubic by increasing  $\beta$ .

### III. LATTICE MODELS AND INTERACTION-INDUCED SHADOW STATES

The emergence of shadow states in the effective continuum model requires (7). It is crucial to examine which microscopic model could lead to effective models as in (1) and (3) and illustrate how these microscopic models map onto the continuum limit discussed in Sec. II. In particular, such microscopic models involve small ratios of NN to NNN hybridizations which would be highly atypical of direct orbital overlaps in a non-interacting model. In

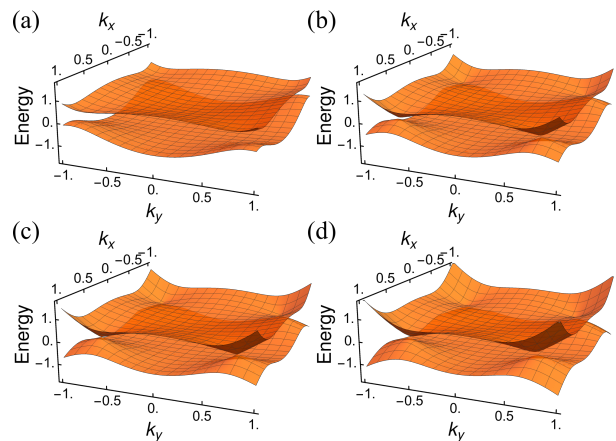


FIG. 3. The bulk band structure for  $\beta = 0.2, 0.3, 1/3, 0.4$  (a-d) at  $k_z = 0$ . The remaining parameters are the same as in Fig. 1. For current parameters  $\beta_c = 1/3$ .

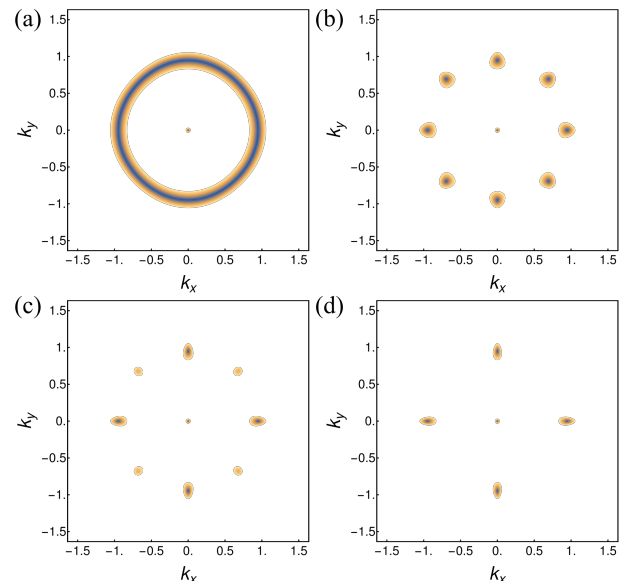


FIG. 4. Density plot of the surface-state gap determined from the numerical solutions for  $\beta = 0.0, 0.2, 0.3, 0.35$  (a-d) respectively. The remaining parameters are the same as in Fig. 1.

this section we show that such hybridization structure can emerge as a result of strong interactions in TKIs.

#### A. General form of the effective hybridization in a lattice model

We consider an effective  $s - p$  orbital hybridization on a three-dimensional lattice in the presence of spin-orbit coupling with the most general tetragonal point-group symmetry. The form of these effective hybridization terms is determined by the point-group symmetry and does not depend on strong correlations. How-

ever, as we discuss in the next section, the effective hybridization gets renormalized due to strong correlations. We consider a general form which allows for tetragonal

anisotropy. The NN and NNN, symmetry-allowed hybridization terms, which include the spin-orbit coupling, in second-quantized form are<sup>39</sup>

$$H_{\text{Hyb}} = \sum_{\mathbf{R}, \mu} \left[ t_{0\parallel} \left( f_{\mathbf{R}\mu}^\dagger \Psi_{0\parallel, \mathbf{R}\mu} + \text{H.c.} \right) + t_{0\perp} \left( f_{\mathbf{R}\mu}^\dagger \Psi_{0\perp, \mathbf{R}\mu} + \text{H.c.} \right) + t_{1\parallel} \left( f_{\mathbf{R}\mu}^\dagger \Psi_{1\parallel, \mathbf{R}\mu} + \text{H.c.} \right) + t_{1\perp} \left( f_{\mathbf{R}\mu}^\dagger \Psi_{1\perp, \mathbf{R}\mu} + \text{H.c.} \right) \right], \quad (8)$$

where  $\mathbf{R}$  labels the sites of the cubic lattice and the  $f_{\mathbf{R}\mu}^\dagger$  operator acts on the lowest-energy Kramers doublet which emerges under the effect of the cubic or tetragonal crystal field from the  $p$ -orbital with spin 1/2. Since the spin is not conserved,  $\mu \in \{1, 2\}$  denotes the two components of the Kramers doublet. We introduced the Wannier states

$$\Psi_{0\parallel, \mathbf{R}\mu} = -\frac{i}{2} \sum_{\hat{\mathbf{r}} \in \{\pm\hat{x}, \pm\hat{y}\}} \sum_{\nu} (\hat{\mathbf{r}} \cdot \boldsymbol{\sigma})_{\mu\nu} c_{\mathbf{R}+\hat{\mathbf{r}}\nu} \quad (9)$$

$$\Psi_{0\perp, \mathbf{R}\mu} = -\frac{i}{2} \sum_{\hat{\mathbf{r}} \in \{\pm\hat{z}\}} \sum_{\nu} (\hat{\mathbf{r}} \cdot \boldsymbol{\sigma})_{\mu\nu} c_{\mathbf{R}+\hat{\mathbf{r}}\nu} \quad (10)$$

$$\Psi_{1\parallel, \mathbf{R}\mu} = -\frac{i}{2} \sum_{\hat{\mathbf{r}} \in \{\pm\hat{x}, \pm\hat{y}\}} \sum_{\nu} (\hat{\mathbf{r}} \cdot \boldsymbol{\sigma})_{\mu\nu} c_{\mathbf{R}+\hat{\mathbf{r}}\nu} \quad (11)$$

$$\Psi_{1\perp, \mathbf{R}\mu} = -\frac{i}{2} \sum_{\hat{\mathbf{r}} \in \left\{ \begin{smallmatrix} \pm\hat{x} \pm \hat{z}, \\ \pm\hat{y} \pm \hat{z} \end{smallmatrix} \right\}} \sum_{\nu} (\hat{\mathbf{r}} \cdot \boldsymbol{\sigma})_{\mu\nu} c_{\mathbf{R}+\hat{\mathbf{r}}\nu}, \quad (12)$$

defined in terms of the  $s$ -orbital, spin-1/2 conduction electrons  $c_{\mathbf{R}\nu}$ . By construction, each of  $\Psi$ 's belong to the same doublet as the  $f$  fermion operators. For the most general tetragonal anisotropy, the NN hybridization splits into in-plane  $t_{0\parallel}$  and out-of-plane  $t_{0\perp}$  contributions, and similarly for the NNN terms  $t_{1\parallel}$  and  $t_{1\perp}$ . Under a straightforward Fourier transformation, the hybridization terms can be re-expressed as:

$$H_{\text{Hyb}} = \sum_{\mathbf{k}, \mu\nu} \left[ V_{0, \mu\nu}(\mathbf{k}) + V_{1, \mu\nu}(\mathbf{k}) \right] f_{\mathbf{k}\mu}^\dagger c_{\mathbf{k}\nu} + \text{H.c.} \quad (13)$$

where

$$V_{0, \mu\nu}(\mathbf{k}) = t_{0\parallel} \sum_{i \in \{x, y\}} s_i \sigma_{i, \mu\nu} + t_{0\perp} \sigma_{z, \mu\nu} s_z \quad (14)$$

$$V_{1, \mu\nu}(\mathbf{k}) = 2 \left[ (t_{1\parallel} c_y + t_{1\perp} c_z) s_x \sigma_x + (t_{1\parallel} c_x + t_{1\perp} c_z) s_y \sigma_y + t_{1\perp} (c_x + c_y) s_z \sigma_z \right] \quad (15)$$

and where  $s_i = \sin(k_i a)$ ,  $c_i = \cos(k_i a)$ .

## B. Continuum limit for cubic symmetry

For cases where the hybridization preserves the cubic point-group symmetry we set  $t_{0\parallel} = t_{0\perp}$  and  $t_{1\parallel} = t_{1\perp}$ . Taking the continuum limit of the hybridization terms in (14) and (15) we arrive at (1) and (3) for  $\beta = 1$  by identifying

$$v = t_0 + 4t_1 \quad (16)$$

$$\alpha v = -t_1, \quad (17)$$

from which the condition for the emergence of shadow states,  $\alpha < -m/M$ , translates into

$$-4t_1 < t_0 < \left( \frac{M}{m} - 4 \right) t_1 \quad \text{if } t_1 > 0 \quad (18)$$

$$\left( \frac{M}{m} - 4 \right) t_1 < t_0 < -4t_1 \quad \text{if } t_1 < 0. \quad (19)$$

## C. Continuum limit for tetragonal symmetry

The parameters of the continuum model in (1) and (3) are related to the lattice model parameters in (14) and 15 via:

$$v_{\parallel} = 2t_{1\parallel} + 2t_{1\perp} + t_{0\parallel}, \quad (20)$$

$$v_{\perp} = t_{0\perp} + 4t_{1\perp}, \quad (21)$$

$$\alpha = \frac{-t_{1\perp}}{t_{0\perp} + 4t_{1\perp}}, \quad (22)$$

$$\beta = \frac{t_{1\parallel}}{t_{1\perp}}, \quad (23)$$

where  $v_{\parallel}$  ( $v_{\perp}$ ) is the hybridization amplitude in the  $xy$  plane and along the  $z$  direction, respectively in (1). As mentioned previously, the anisotropy of the NN hybridization does not have essential consequences.

For tetragonal lattices, the condition for the surface state crossings at finite parallel momentum (the equivalent of (7) when  $v_{\parallel} \neq v_{\perp}$ ) reads as  $\frac{\alpha v_{\perp}}{v_{\parallel}} < -\frac{m}{M}$ . In terms of parameters of tight-binding, the required range

of tight-binding model parameters read as:

$$\frac{-t_{1\perp}}{2t_{1\parallel} + 2t_{1\perp} + t_{0\parallel}} < -\frac{m}{M}. \quad (24)$$

For  $\beta = 0$  ( $t_{1\parallel} = 0$ ), this condition implies

$$-2t_{1\perp} < t_{0\parallel} < \left(\frac{M}{m} - 2\right)t_{1\perp} \quad \text{if } t_{1\perp} > 0 \quad (25)$$

$$\left(\frac{M}{m} - 2\right)t_{1\perp} < t_{0\parallel} < -2t_{1\perp} \quad \text{if } t_{1\perp} < 0. \quad (26)$$

This shows that if  $k_F^2 = M/m < 2$  the emergence of shadow states requires that  $t_{0\parallel}$  and  $t_{1\perp}$  have opposite signs. Recall that this conclusion is a consequence of (24), and is therefore rigorous only in the continuum limit when  $M/m < 1$ . We note that for larger values of  $M/m$ , shadow states could develop even if  $t_{0\parallel}$  and  $t_{1\perp}$  have the same sign. This case corresponds to very large shadow surface state FSs and is consequently relevant in a restricted parameter-space. Therefore, we focus on  $t_{0\parallel}$  and  $t_{1\perp}$  having opposite sign. In Sec.III D we demonstrate that for TKIs and due to the interacting nature of this material, such emergent pattern of parameters is energetically preferred.

#### D. Effective hybridization from Kondo interactions

In this section, we show that  $t_{0\parallel}$  and  $t_{1\perp}$  having opposite signs is energetically preferred at mean-field level for TKIs. In the half-filling limit, we consider the NN and NNN Kondo interaction<sup>40,41</sup>

$$H_K = \sum_{\mathbf{R}} \left[ J_{0\parallel} \mathbf{S}_{0\parallel, \mathbf{R}} \cdot \mathbf{S}_{f, \mathbf{R}} + J_{0\perp} \mathbf{S}_{0\perp, \mathbf{R}} \cdot \mathbf{S}_{f, \mathbf{R}} + J_{1\parallel} \mathbf{S}_{1\parallel, \mathbf{R}} \cdot \mathbf{S}_{f, \mathbf{R}} + J_{1\perp} \mathbf{S}_{1\perp, \mathbf{R}} \cdot \mathbf{S}_{f, \mathbf{R}} \right] \quad (27)$$

where

$$\mathbf{S}_{f, \mathbf{R}} = \frac{1}{2} \sum_{\mu\nu} f_{\mathbf{R}\mu}^\dagger \sigma_{\mu\nu} f_{\mathbf{R}\nu}. \quad (28)$$

For tetragonal symmetry, the in-plane and out-of-plane Kondo couplings are different with  $J_{0/\parallel} \neq J_{0/\perp}$ . Note that the  $f$  fermion is constrained to the half-filled Fock space. Similarly, the operators

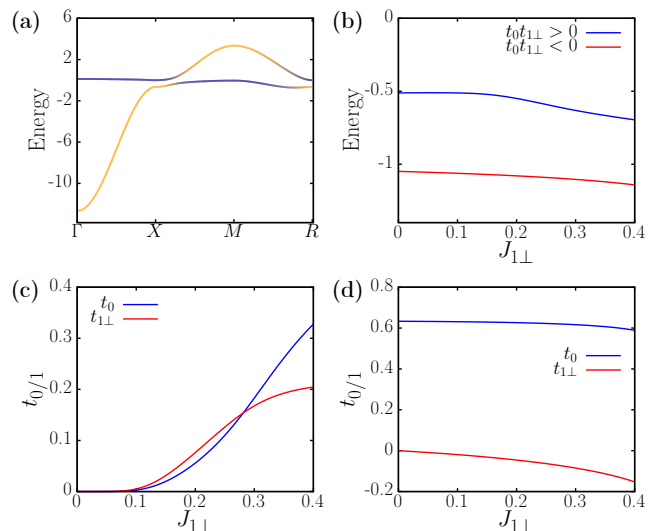


FIG. 5. (a) Band structure determined from (37), (38) and (13) for the self-consistent solutions with effective  $f$ -electron level  $\mu_f = 0.66$ , and NN and NNN hybridization  $t_0 = 0.62$  and  $t_1 = -0.08$ , respectively, which corresponds to  $J_{1\perp} = 0.3$ . Yellow (blue) lines denote  $c(f)$  character. (b) Ground-state energy per unit cell versus NNN Kondo coupling  $J_{1\perp}$  for solutions where the NN and NNN effective hybridizations  $t_0$  and  $t_{1\perp}$ , respectively, have equal (blue line) and opposite (red line) signs. The lowest-energy ground-state configuration occurs when the signs are opposite. Self-consistently determined NN and NNN effective hybridizations  $t_0$  and  $t_{1\perp}$ , respectively, as functions of the NNN Kondo-coupling  $J_{1\perp}$  for (c)  $t_0 t_{1\perp} > 0$  and (d)  $t_0 t_{1\perp} < 0$ . The values of the parameters are:  $t = 1.0$ ,  $t' = 0.5$ ,  $J_{0\parallel} = J_{0\perp} = 1.0$  and  $J_{1\parallel} = 0$ , which correspond to  $t_{0\parallel} = t_{0\perp} = t_0$  and  $t_{1\parallel} = 0$ .

$$\mathbf{S}_{0\parallel, \mathbf{R}} = \frac{1}{2} \sum_{\mu\nu} \Psi_{0\parallel, \mathbf{R}\mu}^\dagger \sigma_{\mu\nu} \Psi_{0\parallel, \mathbf{R}\nu} \quad (29)$$

$$\mathbf{S}_{0\perp, \mathbf{R}} = \frac{1}{2} \sum_{\mu\nu} \Psi_{0\perp, \mathbf{R}\mu}^\dagger \sigma_{\mu\nu} \Psi_{0\perp, \mathbf{R}\nu} \quad (30)$$

$$\mathbf{S}_{1\parallel, \mathbf{R}} = \frac{1}{2} \sum_{\mu\nu} \Psi_{1\parallel, \mathbf{R}\mu}^\dagger \sigma_{\mu\nu} \Psi_{1\parallel, \mathbf{R}\nu} \quad (31)$$

$$\mathbf{S}_{1\perp, \mathbf{R}} = \frac{1}{2} \sum_{\mu\nu} \Psi_{1\perp, \mathbf{R}\mu}^\dagger \sigma_{\mu\nu} \Psi_{1\perp, \mathbf{R}\nu} \quad (32)$$

are defined in terms of the Wannier states in (9)-(12).

A straightforward decoupling of the Kondo interactions in the particle-hole channel reproduces (13) if we identify

$$t_{0\parallel} = -\frac{3J_{0\parallel}}{8} \left\langle \sum_{\mu} \Psi_{0\parallel, \mathbf{R}\mu}^{\dagger} f_{\mathbf{R}\mu} \right\rangle \quad (33)$$

$$t_{0\perp} = -\frac{3J_{0\perp}}{8} \left\langle \sum_{\mu} \Psi_{0\perp, \mathbf{R}\mu}^{\dagger} f_{\mathbf{R}\mu} \right\rangle \quad (34)$$

$$t_{1\parallel} = -\frac{3J_{1\parallel}}{8} \left\langle \sum_{\mu} \Psi_{1\parallel, \mathbf{R}\mu}^{\dagger} f_{\mathbf{R}\mu} \right\rangle \quad (35)$$

$$t_{1\perp} = -\frac{3J_{1\perp}}{8} \left\langle \sum_{\mu} \Psi_{1\perp, \mathbf{R}\mu}^{\dagger} f_{\mathbf{R}\mu} \right\rangle \quad (36)$$

We choose a tight-binding part for conduction and  $f$  electrons<sup>28</sup>:

$$\epsilon_{\mathbf{k}} = -2t \sum_i \cos k_i - 4t' \sum_{i \neq j} \cos k_i \cos k_j, \quad (37)$$

$$\epsilon_{f\mathbf{k}} = -\eta \epsilon_{\mathbf{k}} + \mu_f, \quad (38)$$

where  $\eta = 0.01$  and  $\mu_f$  is the chemical potential for the  $f$  electrons. We impose half-filling for both  $f$  and conduction electrons:

$$1 = \frac{1}{N_k} \left\langle \sum_{\mathbf{k}\mu} f_{\mathbf{k}\mu}^{\dagger} f_{\mathbf{k}\mu} \right\rangle, \quad (39)$$

$$1 = \frac{1}{N_k} \left\langle \sum_{\mathbf{k}\mu} c_{\mathbf{k}\mu}^{\dagger} c_{\mathbf{k}\mu} \right\rangle, \quad (40)$$

where  $N_k$  is the number of points in the bulk BZ. Finally, both  $t_{i\parallel/\perp}$  and  $\mu_f$  are determined self-consistently.

Fig. 5 (a) shows the band structure of the Hamiltonian formed from (37), (38) and (13). The ground state has band inversion at the 3  $M$  points in the in the BZ and therefore has a nontrivial topological  $Z_2$  index. Fig. 5 (b-d) shows the solution of (33-36) for half-filling, when  $t_0 = t_{0\parallel} = t_{0\perp}$  and  $t_{0\parallel} = 0$ . We distinguish solutions with  $t_0$  and  $t_{1\perp}$  having the same and opposite sign. We find that the self-consistent solutions with  $t_0 t_{1\perp} < 0$  minimize the ground-state energy whereas solutions with  $t_0 t_{1\perp} > 0$  are always higher in energy as shown in Fig. 5 (b). Fig. 5 (c) and (d) show the corresponding  $t_{0/\perp}$  as a function of  $J_1$  for  $J_0 = 1$ . At  $J_1 = 0$  the lower energy solution corresponds to finite  $t_0$  and  $t_{1\perp} = 0$ . Moving away to finite  $J_1$

the  $t_0 t_{1\perp} < 0$  solution smoothly connects with that low energy solution, whereas  $t_0 t_{1\perp} > 0$  solution develops in different region and is never preferred.

#### IV. CONCLUSIONS

We showed that, in addition to the Dirac band crossing at the center of the BZ, the surface states of TKIs can also support additional band crossings at generic momenta, provided that the bulk out-of-plane hybridization between quasi-localized and itinerant electrons is dominant. We illustrate that this hybridization realizes the minimum-energy ground-state configuration in TKIs with tetragonal lattice symmetry. In these cases, the topological surface states can have arbitrarily large FSs and hence can mimic the Landau-quantized bulk in quantum oscillation experiments. Our results can provide an alternate explanation for anomalous quantum oscillation experiments in topological insulators with tetragonal symmetry.

#### ACKNOWLEDGEMENT

PG acknowledges support from National Science Foundation Awards No. DMR-1824265 for this work. A.G. acknowledges support from the European Union's Horizon 2020 research and innovation program under the Marie Skłodowska-Curie grant agreement No. 754411. EMN is supported by ASU startup grant. OE is in part supported by NSF-DMR-1904716.

#### V. APPENDIX

In this appendix, we discuss the analytical solutions of the surface states of continuum-limit Hamiltonian  $H_T = H_0 + V_{nm}$  introduced in Sec. II. Taking into account the double-degeneracy of the states due to inversion and time-reversal symmetry, we consider the following two degenerate eigenstates ansatz for the general solutions of  $H_T$  (in the basis  $\{|1, \uparrow\rangle, |2, \uparrow\rangle, |1, \downarrow\rangle, |2, \downarrow\rangle\}$ ,  $\{1, 2\}$  denoting orbital index and  $\{\uparrow, \downarrow\}$  denoting the spin):

$$\psi_{\xi}^1(z) = N_1 \begin{pmatrix} L_- + m_- \lambda_{\xi}^2 - E \\ iv \lambda_{\xi} (1 + \alpha k^2) \\ 0 \\ -vk_x (1 + \alpha (\beta k_y^2 - \lambda_{\xi}^2)) - iv k_y (1 + \alpha (\beta k_x^2 - \lambda_{\xi}^2)) \end{pmatrix} e^{-\lambda_{\xi} z}, \quad (41)$$

$$\psi_{\xi}^2(z) = N_2 \begin{pmatrix} -vk_x (1 + \alpha (\beta k_y^2 - \lambda_{\xi}^2)) + iv k_y (1 + \alpha (\beta k_x^2 - \lambda_{\xi}^2)) \\ 0 \\ -iv \lambda_{\xi} (1 + \alpha k^2) \\ L_+ + m_+ \lambda_{\xi}^2 - E \end{pmatrix} e^{-\lambda_{\xi} z}, \quad (42)$$

where  $L_{\pm} = M_{\pm} - m_{\pm}k_{\parallel}^2$ ,  $M_{\pm} = M' \pm M$ ,  $m_{\pm} = m' \pm m$ ,  $\xi = 1, 2$  and  $\lambda_{\xi}$  are determined from a characteristic equation<sup>36,37</sup>. We focus on non-trivial surface states of a semi-infinite system with an open boundary condition at  $z = 0$  and normalization condition of the wave function in the region  $z > 0$ . Therefore, we are only interested in  $\lambda_{\xi}$  with positive real part. Using the definitions

$$F = m_+(L_- - E) + m_-(L_+ - E) + v^2 \left( 1 + 4\alpha k_{\parallel}^2 + \alpha^2 k_{\parallel}^4 + 4\alpha^2 \beta k_x^2 k_y^2 \right) \quad (43)$$

$$R = F^2 - 4 \left( m_+ m_- - \alpha^2 v^2 k_{\parallel}^2 \right) \times \left[ (L_+ - E)(L_- - E) - v^2 \left( k_{\parallel}^2 + \alpha \beta k_x^2 k_y^2 (4 + \alpha \beta k_{\parallel}^2) \right) \right] \quad (44)$$

we express the solutions via

$$E_{\pm} = \frac{M' m^2 - M m m'}{m^2 + \alpha^2 v^2 k_{\parallel}^2} + \frac{\alpha v^2 \left( m' k_{\parallel}^2 + \alpha \left( M' - m' k_{\parallel}^2 \right) k_{\parallel}^2 + 2\alpha \beta m' k_x^2 k_y^2 \right)}{m^2 + \alpha^2 v^2 k_{\parallel}^2} \pm \frac{v}{m^2 + \alpha^2 v^2 k_{\parallel}^2} \left[ \left( m^2 - m'^2 + \alpha^2 v^2 k_{\parallel}^2 \right) \left( \left( m + \alpha \left( M - m k_{\parallel}^2 \right) \right)^2 k_{\parallel}^2 + \alpha^2 \beta^2 m^2 k_x^2 k_y^2 k_{\parallel}^2 + 4\alpha \beta m k_x^2 k_y^2 \left( m + \alpha \left( M - m k_{\parallel}^2 \right) \right) + \alpha^4 \beta^2 v^2 k_x^2 k_y^2 (k_x^2 - k_y^2)^2 \right) \right]^{1/2}. \quad (48)$$

$$\lambda_{\xi} = \left[ 2 \left( m_+ m_- - \alpha^2 v^2 k_{\parallel}^2 \right) \right]^{-\frac{1}{2}} \times \left( -F + (-1)^{\xi} \sqrt{R} \right)^{\frac{1}{2}} \quad (45)$$

Non-trivial solution satisfying boundary condition at  $z = 0$  are obtained from the requirement  $\det\{\psi_1^1(0), \psi_2^1(0), \psi_1^2(0), \psi_2^2(0)\} = 0$ , which takes simple form at  $k_{2,\parallel}$  when  $\beta = 0$  or  $\theta_k = m\pi/2$ :

$$\lambda_1 \lambda_2 = -\frac{1}{\alpha}, \quad (46)$$

For  $\beta \neq 0$ , and  $\theta_k = \pi/4 + m\pi/2$  also for  $k'_{2,\parallel}$ , the condition is

$$\lambda_1 \lambda_2 = \frac{1}{\beta - 2} \left( \frac{M\beta}{m} + \frac{2}{\alpha} \right). \quad (47)$$

Non-trivial surface states thus require  $\lambda_1 \lambda_2 > 0$  and since  $0 < \beta < 1$ , the above conditions can only be satisfied if  $\alpha < 0$ . In addition, the condition (47) requires  $\alpha > -2m/M\beta$  which is equivalent to  $\beta < \beta_c$  derived in main text.

For general momentum  $k_{\parallel}$ , the non-trivial surface state spectrum is

From this we recover (4) for  $\beta = 0$ .

<sup>1</sup> Z. Fisk, J. L. Sarrao, J. D. Thompson, D. Mandrus, M. F. Hundley, A. Migliori, B. Bucher, Z. Schlessinger, G. Aeppli, E. Bucher, J. F. DiTusa, C. S. Oglesby, H.-R. Ott, P. C. Canfield, and S. E. Brown, *Physica B* **206** & **207**, 798 (1995).

<sup>2</sup> A. Menth, E. Buehler, and T. H. Geballe, *Phys. Rev. Lett.* **22**, 295 (1969).

<sup>3</sup> M. Dzero, K. Sun, V. Galitski, and P. Coleman, *Phys. Rev. Lett.* **104**, 106408 (2010).

<sup>4</sup> M. Dzero, K. Sun, P. Coleman, and V. Galitski, *Phys. Rev. B* **85**, 045130 (2012).

<sup>5</sup> V. Alexandrov, M. Dzero, and P. Coleman, *Phys. Rev. Lett.* **111**, 226403 (2013).

<sup>6</sup> M. Dzero, J. Xia, V. Galitski, and P. Coleman, *Annu. Rev. Condens. Matter Phys.* **7**, 249 (2016).

<sup>7</sup> J. Jiang, S. Li, T. Zhang, Z. Sun, F. Chen, Z. Ye, M. Xu, Q. Ge, S. Tan, X. Niu, M. Xia, B. Xie, Y. Li, X. Chen, H. Wen, and D. Feng, *Nat. Comm.* **4**, 3010 (2013).

<sup>8</sup> D. J. Kim, J. Xia, and Z. Fisk, *Nature Materials* **13**, 466 (2014).

<sup>9</sup> M. Neupane, N. Alidoust, S.-Y. Xu, T. Kondo, Y. Ishida, D. J. Kim, C. Liu, I. Belopolski, Y. J. Jo, T.-R. Chang, H.-T. Jeng, T. Durakiewicz, L. Balicas, H. Lin, A. Bansil, S. Shin, Z. Fisk, and M. Z. Hasan, *Nat. Comm.* **4**, 2991 (2013).

<sup>10</sup> E. Frantzeskakis, N. de Jong, B. Zwartsenberg, Y. K.

- Huang, Y. Pan, X. Zhang, J. X. Zhang, F. X. Zhang, L. H. Bao, O. Tegus, A. Varykhalov, A. de Visser, and M. S. Golden, *Phys. Rev. X* **3**, 041024 (2013).
- <sup>11</sup> J. D. Denlinger, J. W. Allen, J.-S. Kang, K. Sun, B.-I. Min, D.-J. Kim, and Z. Fisk, “Smb<sub>z</sub> photoemission: Past and present,” in *Proceedings of the International Conference on Strongly Correlated Electron Systems (SCES2013)* (2014) p. 017038.
- <sup>12</sup> N. Xu, H. Ding, and M. Shi, *Journal of Physics: Condensed Matter* **28**, 363001 (2016).
- <sup>13</sup> W. A. Phelan, S. M. Koohpayeh, P. Cottingham, J. W. Freeland, J. C. Leiner, C. L. Broholm, and T. M. McQueen, *Phys. Rev. X* **4**, 031012 (2014).
- <sup>14</sup> N. J. Laurita, C. M. Morris, S. M. Koohpayeh, P. F. S. Rosa, W. A. Phelan, Z. Fisk, T. M. McQueen, and N. P. Armitage, *Phys. Rev. B* **94**, 165154 (2016).
- <sup>15</sup> G. Li, Z. Xiang, F. Yu, T. Asaba, B. Lawson, P. Cai, C. Tinsman, A. Berkley, S. Wolgast, Y. S. Eo, D.-J. Kim, C. Kurdak, J. W. Allen, K. Sun, X. H. Chen, Y. Y. Wang, Z. Fisk, and L. Li, *Science* **346**, 1208 (2014).
- <sup>16</sup> B. Tan, Y.-T. Hsu, B. Zeng, M. C. Hatnean, N. Harrison, Z. Zhu, M. Hartstein, M. Kiourlappou, A. Srivastava, M. Johannes, T. P. Murphy, J.-H. Park, L. Balicas, G. G. Lonzarich, G. Balakrishnan, and S. E. Sebastian, *Science* **349**, 287 (2015).
- <sup>17</sup> M. Hartstein, W. Toews, Y.-T. Hsu, B. Zeng, X. Chen, M. C. Hatnean, Q. Zhang, S. Nakamura, A. Padgett, G. Rodway-Gant, J. Berk, M. K. Kingston, G. H. Zhang, M. K. Chan, S. Yamashita, T. Sakakibara, Y. Takano, J.-H. Park, L. Balicas, N. Harrison, N. Shitsevalova, G. Balakrishnan, G. G. Lonzarich, R. W. Hill, M. Sutherland, and S. E. Sebastian, *Nature Physics* **14**, 166 (2018).
- <sup>18</sup> M. Hartstein, H. Liu, Y.-T. Hsu, B. S. Tan, M. C. Hatnean, G. Balakrishnan, and S. E. Sebastian, arXiv preprint arXiv:2007.01453 (2020).
- <sup>19</sup> H. Liu, M. Hartstein, G. J. Wallace, A. J. Davies, M. C. Hatnean, M. D. Johannes, N. Shitsevalova, G. Balakrishnan, and S. E. Sebastian, *Journal of Physics: Condensed Matter* **30**, 16LT01 (2018).
- <sup>20</sup> Z. Xiang, Y. Kasahara, T. Asaba, B. Lawson, C. Tinsman, L. Chen, K. Sugimoto, S. Kawaguchi, Y. Sato, G. Li, S. Yao, Y. L. Chen, F. Iga, J. Singleton, Y. Matsuda, and L. Li, *Science* **362**, 65 (2018).
- <sup>21</sup> J. Knolle and N. R. Cooper, *Phys. Rev. Lett.* **115**, 146401 (2015).
- <sup>22</sup> J. Knolle and N. R. Cooper, *Phys. Rev. Lett.* **118**, 096604 (2017).
- <sup>23</sup> B. Skinner, *Phys. Rev. Materials* **3**, 104601 (2019).
- <sup>24</sup> G. Baskaran, ArXiv e-prints (2015), arXiv:1507.03477.
- <sup>25</sup> O. Erten, P.-Y. Chang, P. Coleman, and A. M. Tsvelik, *Phys. Rev. Lett.* **119**, 057603 (2017).
- <sup>26</sup> D. Chowdhury, I. Sodemann, and T. Senthil, *Nat Commun.* **9**, 1766 (2018).
- <sup>27</sup> C. M. Varma, arXiv , 2008.07042 (2020).
- <sup>28</sup> V. Alexandrov, P. Coleman, and O. Erten, *Phys. Rev. Lett.* **114**, 177202 (2015).
- <sup>29</sup> O. Erten, P. Ghaemi, and P. Coleman, *Phys. Rev. Lett.* **116**, 046403 (2016).
- <sup>30</sup> L. Fu, *Phys. Rev. Lett.* **103**, 266801 (2009).
- <sup>31</sup> F. Schindler, A. M. Cook, M. G. Vergniory, Z. Wang, S. S. P. Parkin, B. A. Bernevig, and T. Neupert, *Science Advances* **4** (2018), 10.1126/sciadv.aat0346, <https://advances.sciencemag.org/content/4/6/eaat0346.full.pdf>.
- <sup>32</sup> X.-L. Qi and S.-C. Zhang, *Rev. Mod. Phys.* **83**, 1057 (2011).
- <sup>33</sup> H. Zhang, C.-X. Liu, X.-L. Qi, X. Dai, Z. Fang, and S.-C. Zhang, *Nature physics* **5**, 438 (2009).
- <sup>34</sup> C.-X. Liu, X.-L. Qi, H. Zhang, X. Dai, Z. Fang, and S.-C. Zhang, *Phys. Rev. B* **82**, 045122 (2010).
- <sup>35</sup> W. Zhang, R. Yu, H.-J. Zhang, X. Dai, and Z. Fang, *New Journal of Physics* **12**, 065013 (2010).
- <sup>36</sup> W.-Y. Shan, H.-Z. Lu, and S.-Q. Shen, *New J. Phys.* **12**, 043048 (2010).
- <sup>37</sup> S.-Q. Shen, *Topological insulators*, Vol. 174 (Springer, 2012).
- <sup>38</sup> W. P. Su, J. R. Schrieffer, and A. J. Heeger, *Phys. Rev. B* **22**, 2099 (1980).
- <sup>39</sup> P. Coleman, *Introduction to many-body physics* (Cambridge University Press, 2015).
- <sup>40</sup> P. Ghaemi and T. Senthil, *Phys. Rev. B* **75**, 144412 (2007).
- <sup>41</sup> P. Ghaemi, T. Senthil, and P. Coleman, *Phys. Rev. B* **77**, 245108 (2008).